Rate of Formation of Oblique Shock Waves

D. Weihs* and C. J. Freitas†
Southwest Research Institute, San Antonio, Texas 78229

Introduction

OBLIQUE shock waves are obtained when a finite disturbance of topologically compact support, such as a finite body, moves through a compressible medium at supersonic speeds, causing a deflection of the flow within certain limits. The steady solutions of the equations of motion are well known[1] and indicate the existence of two families of steady oblique shock waves, strong and weak shocks, respectively. These are either attached to the leading edge, or blend into a normal shock ahead of the body, depending on the leading-edge shape and body speed. The process involved in the formation of these shocks during the transient starting period and its duration are less well understood and will be examined in the present paper.

Such starting transients appear in various practical problems, such as starting loads on wind-tunnel models in blow-down type tunnels,[2] the loads on artillery shells as they emerge from the barrel, and the sudden deflection of aircraft control surfaces while in supersonic flight.

A different configuration, in which the speed of shock formation has an important effect, occurs when a cascade of airfoils that is moving sideways (the Cartesian equivalent of rotation) encounters an oblique shock. Figure 1 shows the changes in the flowfield at different times for this configuration.

At frame 1 (indicated by ray 1), the shock is undisturbed, and the flow is deflected uniformly following the shock. At frame 2 (ray 2), the rear part of blade A has encountered the shock and some of the shock is reflected (marked as ray 2′), as the flow on A is parallel to A. Another part of the original shock ray 2 still exists further downstream, since the information about the existence of blade A has not yet reached it. This is marked as ray 2″. Frames 3 and 4 are similar to 2, except that the regions of deflected flow have grown. The present study will determine the rate of this growth. Frame 5 again shows an undisturbed shock, but this has only a finite length, as its influence has only started, a short time before. The "tail" of shock ray 5 is still moving above A. Frames 6 and 7 are equivalent to rays 2 and 3, while frame 8 shows why the cut-off tail of the shock rays just mentioned is important, because it can impact the underside of the previous blade in the row, producing a new reflection (8‴).

Analysis

In the present Note, we analyze a relatively simple configuration that allows for an analytic solution and includes all of the significant factors involved in this type of phenomena. This is a two-dimensional wedge of opening angle 2δ, in quiescent air, that at time $t=0$ is suddenly and instantaneously accelerated to a supersonic speed of Mach number M_1, where $M_1>1$. The ambient air is considered an ideal, thermally perfect gas with $\gamma=1.4$, and the flow away from the shock is taken as isentropic. This model problem can be shown to be essentially equivalent, under Galilean transformations, to the physical cases just discussed.

The steady-state solution is, as just mentioned, known (Ref. 1, Chap. 16). We limit ourselves to the range of parameters where the steady solution is obtained as an oblique *attached* wave and analyze the process leading to its formation. The strong solution, which is obtained when there are large externally forces pressure gradients, is not considered at present. The aforementioned wedge flow has geometrical self-similar qualities, thus enabling an analytical solution.

At each point on the *surface* of the wedge, the flow is being deflected to move in a direction parallel to the surface, starting at the same time $t=0$. To analyze the flow, we look at a point N, situated at an arbitrary distance L from the wedge vertex (see Fig. 2). The flow is deflected at this point beginning at $t=0$, so that local conditions equal to those following a steady oblique shock are obtained. Information about the flow deflection moves away from the point N as a shock. While moving, these pressure signal are swept downstream at speed u_2. The signal from point N that reaches the equilibrium shock position at point Q in the shortest time is moving at an angle β to the wedge surface. The angle β is obtained by minimizing, as a function of angle α, the time elapsed until the signal from N first reaches the oblique shock location, measured from the wedge surface. Note that while each point on the wedge surface, such as N, produces a cylindrical shock that would decay with distance, the fact that all the points on the wedge produce identical shocks results in a plane moving shock, such as that described in Ref. 1 (Chap. 25).

From Fig. 2, we see that the components of signal velocity V, normal to and parallel to the wedge surface, can be written as a function of the pressure wave direction in the form

$$V\sin\beta = W\sin\alpha \tag{1}$$

$$V\cos\beta = W\cos\alpha + u_2 \tag{2}$$

where W is the speed of a moving shock that causes a pressure ratio P_2/P_1 to be produced across it. The pressure ratio is

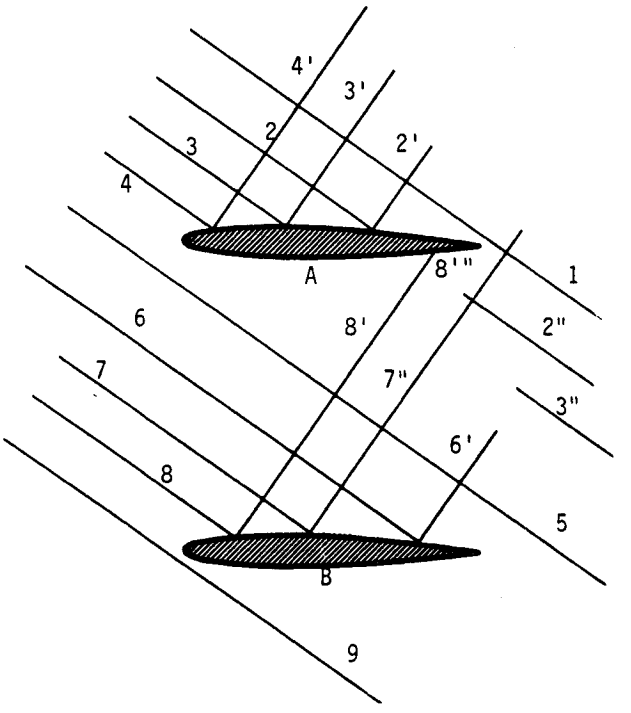

Fig. 1 Schematic drawing of temporal evolution of the flowfield in the region of an oblique shock interacting with two moving cascade blades. Numbers indicate shock position at consecutive times. A single prime indicates primary reflections, a double prime continuation of unreflected shocks, and a triple prime secondary reflections.

Received May 7, 1990; accepted for publication July 24, 1990.

*Visiting Scientist, Department of Fluid Systems; permanent position, Professor, Faculty of Aerospace Engineering, Technion, Haifa 32000, Israel.
†Senior Research Engineer.

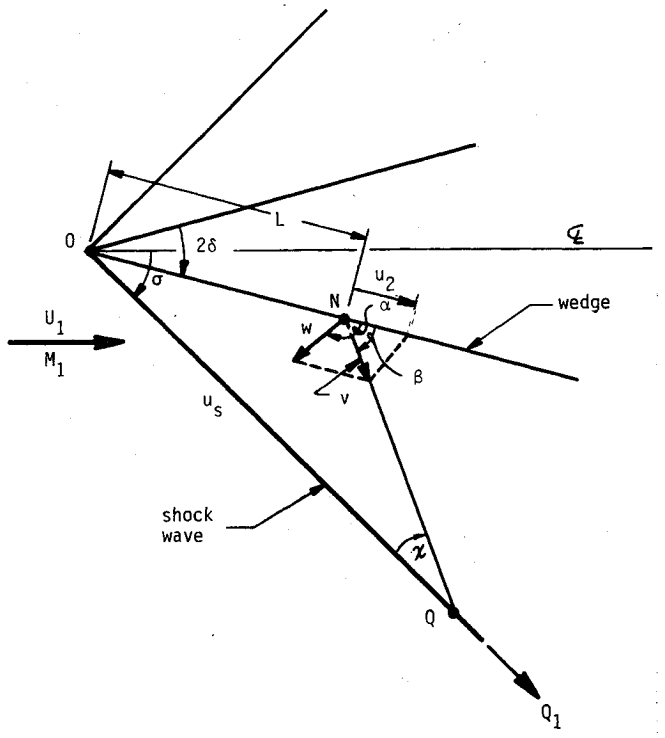

Fig. 2 Wedge flow geometry and velocities.

taken as the final steady pressure ratio, i.e., the full change occurs at the surface. This pressure ratio is[1]

$$\frac{P_2}{P_1} = 1 + \frac{2\gamma}{\gamma+1}\left[\left(\frac{W}{c_1}\right)^2 - 1\right] \tag{3}$$

where 1 and 2 stand for conditions upstream and downstream of the steady oblique shock, P is the pressure, c the speed of sound, γ the ratio of specific heats of the gas ($\gamma = 1.4$ in our calculations).

Applying trigonometric relations to the triangle ONQ, we can obtain the shock formation speed u_s (or more generally, M_s). The argument is that the signal from an arbitrary point N crosses the equilibrium shock OQ_1 earliest at point Q. Thus, due to similarity, the shock will appear at distance $\overline{OQ}$ from O at time τ, which is obtained by

$$V\tau = \overline{NQ} \tag{4}$$

so that the speed of formation, which is constant, again due to geometrical similarity, is defined by

$$u_s\tau = \overline{OQ} \tag{5}$$

The sine theorem for triangle ONQ results in

$$\frac{\overline{ON}}{\sin\xi} = \frac{\overline{NQ}}{\sin(\sigma=\delta)}$$

or

$$\frac{L}{\sin[\beta-(\sigma-\delta)]} = \frac{V\tau}{\sin(\sigma-\delta)} \tag{6}$$

from which we can obtain the time τ by substituting Eq. (1) and Eq. (2) with Eq. (3) into Eq. (6). This results in

$$\tau = \frac{L\sin(\sigma-\delta)}{c_1\sin\alpha\cos(\sigma-\delta) - (c_1\cos\alpha + u_2)\sin(\sigma-\delta)} \tag{7}$$

and to find the ray that crosses $\overline{OQ}$, in the minimum time, we take the derivative $\partial\tau/\partial\alpha$ for fixed L, c_1, $\sigma-\delta$, u_2 (given incoming flow and wedge deflection angle). The fastest traverse occurs when

$$\tan\alpha = -\frac{1}{\tan(\sigma-\delta)} \tag{8}$$

i.e., the ray emanating at an angle α from N that satisfied Eq. (8) reaches the line $\overline{OQ_1}$ first. Next, we calculate the shock speed by again using the sine-theorem

$$\frac{V\tau}{\sin(\sigma-\delta)} = \frac{u_s\tau}{\sin(180\text{ deg}-\beta)} \tag{9}$$

and substituting Eq. (1) into Eq. (9) and simplifying the resulting expression. We have for the shock speed

$$u_s = W\frac{\sin\alpha}{\sin(\sigma-\delta)} \tag{10}$$

or dividing by c_1

$$M_s = \frac{W}{c_1}\frac{\sin\alpha}{\sin(\sigma-\delta)} \tag{11}$$

Next, we relate the shock angle σ to the given external conditions M_1 and the wedge semiangle δ by applying the Rankine-Hugoniot and Prandtl relationships for steady oblique shocks.[1] Using the steady flow relations is permissible as the shock angle σ is the only parameter required here By applying the isentropic relations[1]

$$\frac{P_2}{P_1} = 1 + \gamma M_1^2\sin^2\sigma\left(1-\frac{\rho_1}{\rho_2}\right) \tag{12}$$

$$\frac{P_1}{P_2} = \frac{[(\gamma+1)/(\gamma-1)](\rho_2/\rho_1)-1}{(\gamma+1)/(\gamma-1)-(\rho_2/\rho_1)} \tag{13}$$

$$\frac{\rho_1}{\rho_2} = \frac{\tan(\sigma-\delta)}{\tan\sigma} \tag{14}$$

the angle σ is obtained as a function of δ and M_1. Substituting these relations and Eq. (8) into Eq. (11) gives the shock formation speed as a function of these two parameters only [we will not write out the final unwieldy explicit functional form $M_s = M_s(M_1, \delta)$ to conserve space]. In practice, it is easier to compute M_s through the sequential solution of these equations, i.e, (8) and (11-14). These equations constitute five relations between the seven variables P_2/P_1, ρ_2/ρ_1, M_1, δ, σ, α, and M_s. Any two of these variables, therefore, may be taken as independent parameters, the values of which completely determine the values of the remaining five variables.

Results

Performing the calculations for various deflection angles δ and incoming Mach number M_1, we obtain Fig. 3, which shows the ratio of shock formation Mach number M_s to M_1 vs the deflection angle δ, for various values of M_1. For each value of M_1, only a limited range of deflection angles is shown, as for higher angles, the shock is detached and curved, and requires a different analysis. The shock Mach number is seen to go through a maximal value, different for each M_1. This maximum can be explained by the fact that there are two "competing" effects that influence formation speed. These are shock strength, which goes *up* as δ increases for given M_1, and shock angle σ that translates here into the distance $\overline{NQ}$, which goes *down* as δ increases. It may also be related to the fact that in steady flow, for $\gamma = 1.4$ there is a narrow range of conditions close to the maximum angle for attached shocks, where the flow behind the shock is subsonic. Other manifestations of this "different" region can be seen in oblique shock charts where the pressure ratio goes through its extremal values for deflec-

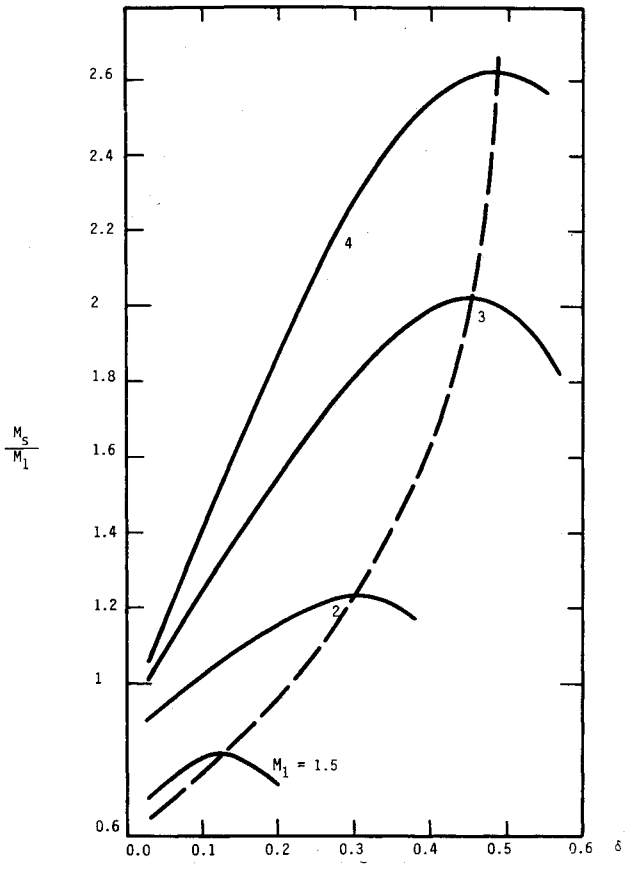

Fig. 3 The ratio of shock formation speed M_s to upstream Mach number M_1 vs wedge semiangle δ (in radians), for various values of M_1. A broken line indicates maximal formation speed. Curves end when an attached shock does not exists (large δ).

tion angles slightly less than the maximum angle for attached shock waves.

Further study of these unsteady formation and cancellation phenomena for the more complex flowfields such as that of Fig. 1 is underway at the present and will be reported in due course.

References

[1]Shapiro, A. H., *The Dynamics and Thermodynamics of Compressible Fluid Flow*, Ronald, New York, 1953, Vols. 1 & 2, p. 1185.

[2]Pope, A., and Goin, K. L., *High Speed Wind Tunnel Testing*, Wiley, New York, 1968, p. 474.

Analysis of ASTM D 3410 Compression Test Specimens

Seng C. Tan*
Wright Materials Research, Dayton, Ohio 45433

Introduction

THE existing compression test methods for composite laminates can be classified into four main categories: end-loaded straight coupon, face-loaded straight coupon, point-loaded sandwich beam, and radial-loaded ring specimen. The methods in the first three categories have been utilized extensively. Unfortunately, the compressive strengths of unidirectional composites measured by different test methods vary significantly.[1-5] The diversity could be attributed to the fact that the stress concentrations in the specimens are significantly different using different test methods. In addition, stability could be a problem for some of the test methods.

Two of the most commonly used compression test methods are the Test Method for Compressive Properties of Unidirectional or Crossply Fiber-Resin Composites (D 3410-87),[6] which are standard test methods utilized by the American Society for Testing and Materials (ASTM). The standard ASTM D 3410 includes the Celanese and the Illinois Institute of Technology Research Institute (IITRI) test methods. The main difference between these two methods is the grip design of the fixtures. The grip construction restricts the overall tabbed specimen thickness of the Celanese test to around 0.157 in. (3.99 mm), whereas the overall tabbed specimen thickness of the IITRI test can be anywhere from 0.059 in. (1.5 mm) to 0.5 in (12.7 mm).

To the author's knowledge, there is no analysis available for the Celanese and the IITRI test methods in the open literature. The small unsupported gauge length of the Celanese and IITRI test specimens [both are 0.5 in. (12.7 mm)] has created a concern that the stress distribution in the specimen may not be uniform. Therefore, the objective of this study is to analyze these compression test specimens.

Formulation

A schematic diagram of the Celanese gripping device is illustrated in Fig. 1. The parameter P denotes the applied load, and R designates the reaction force acting in a ϕ degree direction clockwise from the normal direction of the matching slanted surfaces. The normal and shear load applied at the end tab of the specimen are denoted by N and S, respectively. According to the friction law, the following relation is obtained:

$$\mu = \tan\phi = F/W \tag{1}$$

where μ is the friction coefficient between the contact surfaces. The parameter F is the force required to move one surface over another, and W is the force pressing the surfaces together. The value of μ for clean steel on steel is 0.58 (Ref. 7). Using this value the angle ϕ can be calculated as

$$\phi = \tan^{-1}\mu = 30.11 \text{ deg} \tag{2}$$

Considering the force equilibrium in the vertical direction of Fig. 1a;

$$R = \frac{P}{\sin(10+\phi)} \tag{3}$$

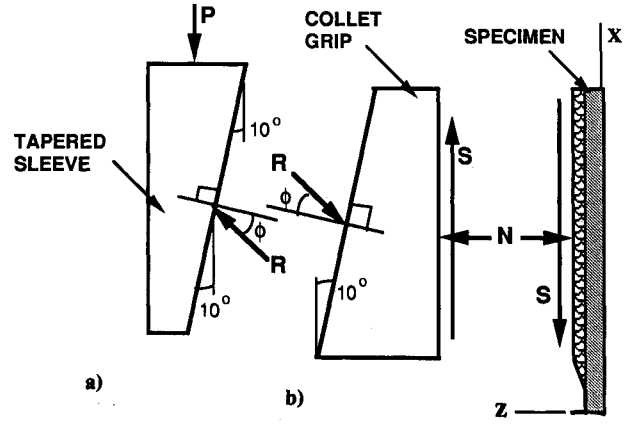

Fig. 1 Load transfer mechanisms between Celanese fixture and specimen.

Received May 31, 1990; revision received June 25, 1990; accepted July 5, 1990.

*Senior Research Scientist (on-site contractor), Air Force Materials Laboratory, WRDC/MLBM, Wright Patterson AFB; currently at Northwestern University, Evanston, IL 60298. Member AIAA.